REFRACTION INDEX OF ELLIPTIC DOUBLE QUANTUM RINGS IN MAGNETIC FIELD

Doina BEJAN[1], Cristina STAN[2]*

We present a theoretical study focused on the influence on the refractive index of the geometry variation of the interior ring of a GaAs/GaAlAs concentric double quantum ring structure in the presence of a constant, uniform magnetic field. Changing the boundaries form of the interior ring from circles to ellipses, new electronic properties and various refractive indexes can be obtained and adjusted accordingly.

Keywords: quantum ring, magnetic field, refraction index

1. Introduction

In the last two decades, studies on the properties of semiconductor nanostructures in different ring type configurations from simple to multiple, circular, or elliptical, horizontally, or vertically coupled are subjects of high interest for scientific communities, both experimentalists and theorists [1-9]. The effect of magnetic field on such structures with and without a donor impurity is an important issue due to the special confinement of electrons, evidence of Aharonov-Bohm oscillations and the possibility of manipulation of the electrical and optical properties, as reported in [10-19].

Previously, we published extensive studies on the influence of the superposed action of the deformation of the double quantum ring (DQR) geometry, with and without the presence of a donor impurity, and the variation of the external magnetic field on the DQR electronic and absorption spectra [20,21].

In this paper we present a study focused only on the effects produced by the geometry deformation of the interior ring of a concentric DQR semiconductor

[1] Assoc. Prof., Faculty of Physics, University of Bucharest, Bucharest, Romania, e-mail: doinitabejan@yahoo.com

[2]* Prof., Faculty of Applied Sciences, University POLITEHNICA of Bucharest, Bucharest, Romania, e-mail: cristina.stan@upb.ro

structure placed in a constant, uniform, external magnetic field. We theoretically investigate and physically explain the modifications observed in the energy spectra. Also, we compute the relative variation of the refraction index – as a useful measurable quantity, reflecting the response of the system to the probe laser and magnetic field.

The paper is organized as follows. In Section 2 we describe the theoretical framework. The electronic and optical properties are presented and analyzed in Section 3. Finally, the conclusions are summarized in Section 4.

2. Theory

The Hamiltonian for a conduction band electron in a double quantum ring subjected to a magnetic field oriented perpendicular to the rings plane [20] is expressed as:

$$H_0 = \frac{\hbar^2 k^2}{2m^*} + V_1(x,y) + V_2(z) \tag{1}$$

where $\vec{k} = -i\nabla + e\vec{A}/\hbar$ with $\vec{A} = B/2(-y,x,0)$ is the potential vector in the Coulomb gauge ($\nabla\vec{A} = 0$), m^* - the effective mass and e - the absolute value of the electron charge. The in-plane confinement potential $V_1(x,y)$ is rectangular, with zero amplitude in the two rings zones and V_0 elsewhere. The first ring is delimited by (R_1,R_2) and the second one by (R_3,R_4) values. We also use different effective masses of electron in the (x,y) plane: m_{GaAs} in the rings region and m_{AlGaAs} outside.

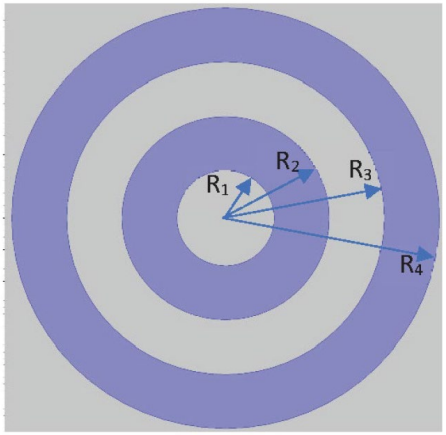

Fig.1 Geometrical (in-plane) structure of the double quantum ring (DQR)

We consider various in-plane deformation of the interior ring on x and y directions, with (R_{1x}, R_{1y}) and

(R_{2x}, R_{2y}) semi-axes of the inner and outer ellipses, respectively. In all further computations, the radiuses R_3 and R_4 of the outer ring are kept unchanged.

In our approximation, both rings have the same height, smaller than the rings width, allowing the decoupling of the in-plane and vertical motions. Therefore, the in-plane movement of electron is described by the Hamiltonian:

$$H_{0||} = -\frac{\hbar^2}{2m*}\left(\frac{\partial^2}{\partial x^2}+\frac{\partial^2}{\partial y^2}\right)+\frac{ieB}{2m*}\left(y\frac{\partial}{\partial x}-x\frac{\partial}{\partial y}\right)+\frac{e^2B^2}{8m*}\left(x^2+y^2\right)+V_1(x,y)\ . \tag{2}$$

Equations are numerically solved using a finite element method [22] in a square geometry using Dirichlet boundary condition.

To describe the refraction index of the DQR, we make use of the Paspalakis *et al*. [23] approximation for the susceptibility induced by a probe laser:

$$\begin{aligned}\chi(\omega) &= i\,Im(\chi)+Re(\chi)= \\ &\frac{iNe^2\mu_{ij}^2T_2}{\varepsilon_0\hbar}\frac{\left|J_0^2\left(\frac{|\mu_{jj}-\mu_{ii}|eE_0}{\hbar\omega}\right)-J_2^2\left(\frac{|\mu_{jj}-\mu_{ii}|eE_0}{\hbar\omega}\right)\right|}{1+T_2^2(\omega-\omega_{ji})^2+\overline{\mu}_{12}^2E_0^2T_1T_2/\hbar^2} \\ &-\frac{Ne^2\mu_{ij}^2E_0T_2^2(\omega-\omega_{ji})^2}{\varepsilon_0\hbar}\frac{\left(J_0\left(\frac{|\mu_{jj}-\mu_{ii}|eE_0}{\hbar\omega}\right)+J_2\left(\frac{|\mu_{jj}-\mu_{ii}|eE_0}{\hbar\omega}\right)\right)^2}{1+T_2^2(\omega-\omega_{ji})^2+\overline{\mu}_{ij}^2E_0^2T_1T_2/\hbar^2}\end{aligned} \tag{3}$$

where, ω is the angular frequency and E_0 the amplitude of the electric field of the probe laser, $\omega_{ji}=\frac{E_j-E_i}{\hbar}$, J_0, J_2 are the ordinary Bessel functions of order 0 and 2, T_1 is the population decay time and T_2 the dephasing time, ε_0 is the vacuum permittivity. Also,

$$\overline{\mu}_{ij}=\mu_{ij}\left(J_0\left(\frac{|\mu_{jj}-\mu_{ii}|eE_0}{\hbar\omega}\right)+J_2\left(\frac{|\mu_{jj}-\mu_{ii}|eE_0}{\hbar\omega}\right)\right) \tag{4}$$

where the electric dipole matrix elements are specifically defined as:

$$\mu_{ij} = \left\langle \Psi_i(x,y) \middle| x \middle| \Psi_j(x,y) \right\rangle \tag{5}$$

for a probe laser polarized along the *x*-axis.

The above susceptibility that gives rise to the complex refraction index:

$$\left(n_T(\omega) + i\kappa(\omega)\right)^2 = n_r^2 + \chi(\omega) \tag{6}$$

where n_r is the static refractive index of the material. Comparison of the real and imaginary parts of Eq. (6) yields the system of equations:

$$n_T^2 - \kappa^2 = n_r^2 + \mathrm{Re}(\chi), \qquad 2n_T\kappa = \mathrm{Im}(\chi), \tag{7}$$

that, for small values of $Im(\chi), Re(\chi)$ can be approximated to:

$$n_T = n_r + \frac{Re(\chi)}{2n_r}, \qquad \kappa = \frac{Im(\chi)}{2n_T}. \tag{8}$$

3. Results and discussion

The numerical values used in our computations are: $m^*_{GaAs} = 0.067 \cdot m_0$, $m^*_{GaAlAs} = 0.0919 \cdot m_0$, ε_r=12.65, V_0=228 meV (for GaAs/$Ga_{0.7}Al_{0.3}As$). For the rings parameters we choose: R_{1x}=15 nm, R_{1y} variable from 6 nm to 15 nm, R_{2x}=32 nm, R_{2y} variable from 32 nm to 42 nm, R_3=49 nm and R_4=66 nm, $N = 5 \cdot 10^{21} m^{-3}$ and temperature T=4K. For the probe laser we consider $E_0 = 4.6 \cdot 10^4$ V/m corresponding to an intensity I_0=10^7W/m^2.

3.1 Electronic properties of the double ring in magnetic field

We are interested in the modifications induced in the electronic properties of DQR by the deformation of the interior ring, in the presence of an external, constant magnetic field. A first geometry of interest is created by varying the R_{1y} semi-axis while keeping R_{1x}, R_{2x}, R_{2y} constants with R_{1x}=15 nm and R_{2x}=R_{2y}=32 nm. In such configuration, the interior ring is bounded by an inner ellipse and an outer circle.

Figure 2 shows the energy spectrum of the lowest six energy levels of an electron confined in the DQR, when R_{1y} semi-axis is increased, at a constant value of

the magnetic field, B=10 T, together with the *x*-*y* projections of some wave-functions (WFs) that help the explanation of the spectrum.

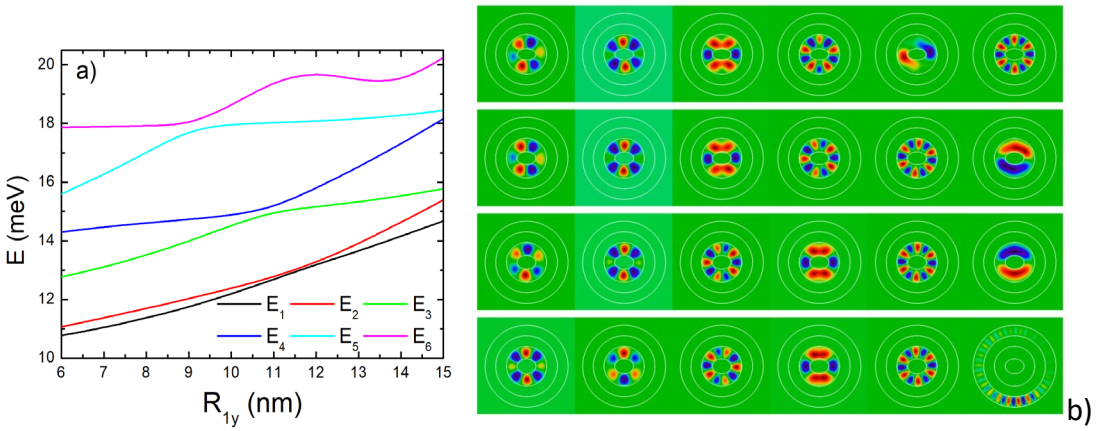

Fig. 2 a) The energy spectrum versus R_{1y} for the lowest six states at B=10T; b) the *x*-*y* projections of the WFs ordered in the increasing value of the energy for R_{1y}=9, 10, 11, 12 nm, from top to bottom.

The graph in Fig.2a shows that the levels are well separated and have a specific dependence on R_{1y}, showing three avoided crossings. Due to the strong confinement of the electron in the interior ring induced by the magnetic field, the anti-crossings can be explained by the exchange of symmetry between the wave functions. This behaviour is totally different from the case of B=0, studied in [20] where the electron densities of some energy levels were placed on the outer ring.

At the increment of R_{1y}, the first anti-crossing in Fig.2a can be seen around R_{1y}=9.2 nm, with a large energy separation between E_5 and E_6. This is because WF_6 for R_{1y}=9 nm (Fig. 2b, first row), a function with many lobes and symmetric to both *x* and *y*-axes, becomes WF_5 for R_{1y}=10 nm (Fig. 2b, second row), but WF_5 (R_{1y}=9 nm) is slightly different from WF_6 (R_{1y}=10 nm). A second anti-crossing, between E_3 and E_4, around R_{1y}=11 nm, can be explained based on a similar argumentation, of the exchange in the symmetry between WF_3 and WF_4 (Fig. 2b, second and third row). A third anti-crossing appears between E_1 and E_2 around R_{1y}=11.5 nm, induced by symmetry change between WF_1 and WF_2. For R_{1y}=11 nm (Fig. 2b, third row), WF_1 is symmetric only to *y*-axis but WF_2 is symmetric to both *x* and *y*-axes while for R_{1y}=12 nm (Fig. 2b, fourth row), their symmetry is reversed.

Other geometry of interest consists in a configuration with the interior ring bounded by two ellipses having the largest semi-axes oriented perpendicularly. This is obtained by the variation of the R_{2y} semi-axis for fixed values of the R_{1y}.

Figure 3 illustrates the variation of the lowest six energy levels at R_{2y} increment, in the presence of the magnetic field, for three values of R_{1y}.

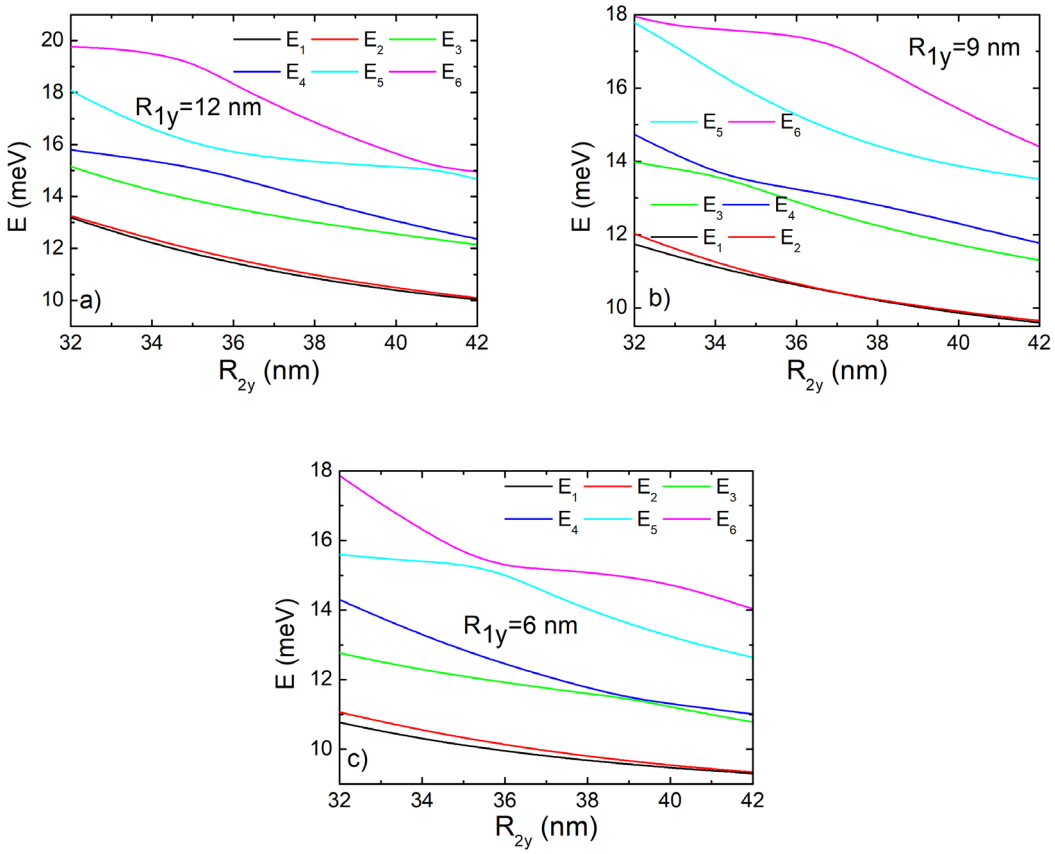

Fig. 3 The energy spectrum versus R_{2y} for the lowest six states, at B=10T: a) R_{1y}=12 nm; b) R_{1y}=9 nm; c) R_{1y}=6nm.

As a general observation, all energies decrease at R_{2y} increment. Also, an increasing number of avoided crossings can be seen in each spectrum at R_{1y} decrement. For instance, the DQR with R_{1y}=12 nm shows only one anti-crossing between E_5 and E_6 around R_{1y} =41 nm due to the change of symmetry between WF_5

and WF_6 that can be observed in Fig. 4a. The levels E_1 and E_2 are almost superposed having similar electron densities.

For the DQR with R_{1y}=9 nm there are two avoided crossings: one between E_3 and E_4 around R_{2y}=34 nm and another between E_1 and E_2 around R_{2y}=37 nm. The exchange of symmetry between WF_1 and WF_2 can be clearly seen in Fig. 4b. Passing from R_{2y}=36 nm to R_{2y}=38 nm, WF_1 (R_{2y}=38 nm) takes the symmetry of WF_2 (R_{2y}=36 nm) but WF_2 (R_{2y}=38 nm) has a symmetry different from WF_1 (R_{2y}=36 nm). The exchange of symmetry between WF_3 and WF_4 can be also easily seen by comparing the first row of Fig. 4b with the first row of Fig. 2b. For the DQR with R_{1y}=6 nm a third avoided crossings takes place between E_5 and E_6 and can be similarly interpreted (not represented here since its WFs are similar to the other cases).

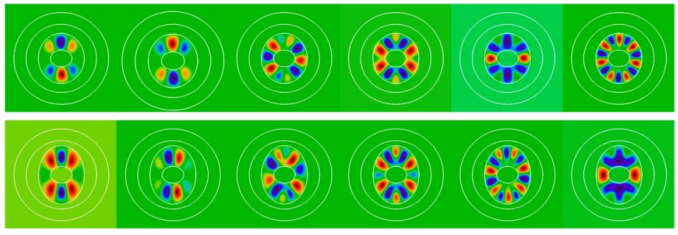
a)

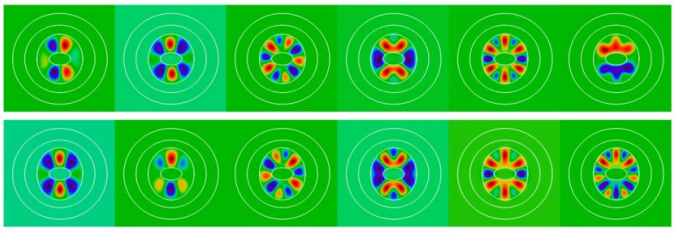
b)

Fig. 4 The *x*-*y* projections of the WFs at B=10 T, ordered in the increasing value of the energy: a) for R_{1y}=12 nm, R_{2y}=36 nm upper row, R_{2y} =42 nm bottom row; b) R_{1y} =9 nm, R_{2y} =36 nm upper row, R_{2y} =38 nm bottom row.

3.2. Influence of geometry on the refraction index

The deformations of the DQR structure also influence the optical properties. Useful information on the changes in the optical properties of the DQR in the presence of a static magnetic field can be obtained from the values of the relative variation of the refractive index:

$$\frac{\Delta n_r}{n_r} = \frac{Re(\chi)}{2n_r^2}. \tag{9}$$

At the chosen intensity of the probe laser, $J_0 = 1, J_2 = 0$ at all photon energies so $Re(\chi)$ is mostly influenced by dipole transition moments μ_{ij}. Therefore, for a proper phenomenological interpretation of the relative variation of the refractive index, we firstly analyze the absolute values of the dipole moments showed in Fig.5.

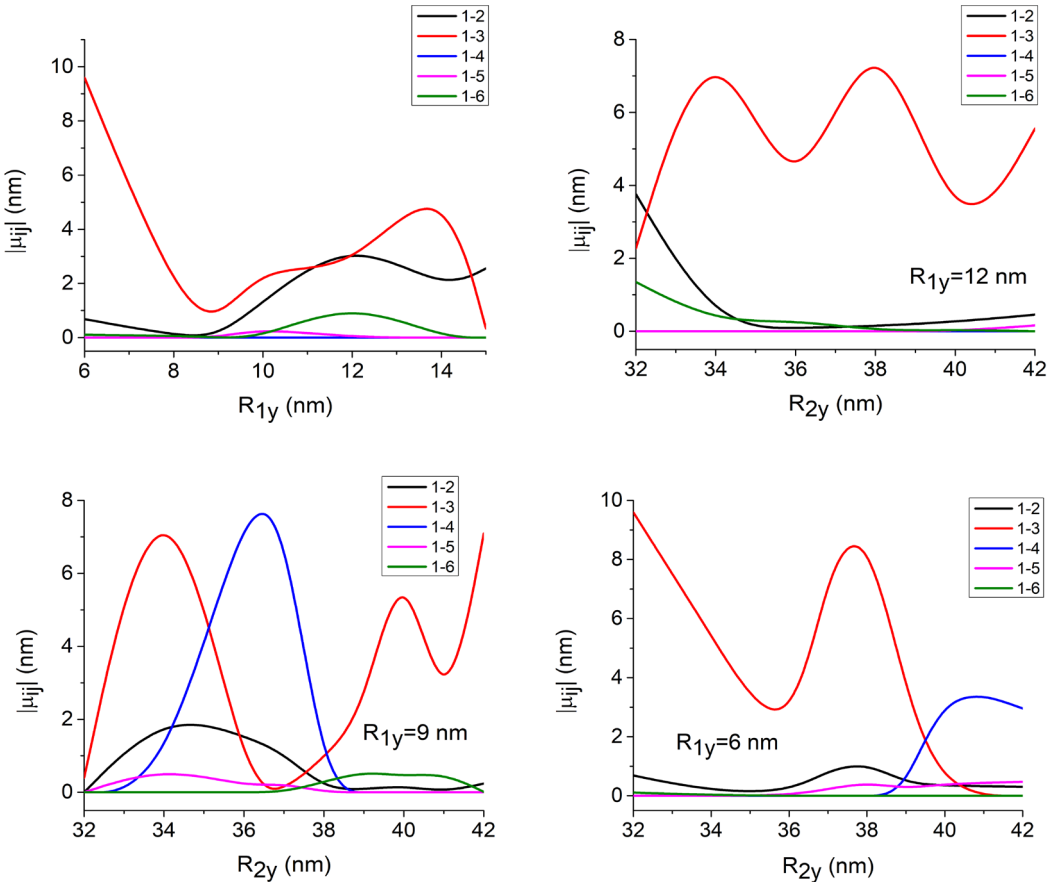

Fig. 5 The absolute values of the dipole moments of DQR at B=10T: for different values of R_{1y} and R_{2y} = 32 nm; and for different values of R_{2y} for R_{1y} = 12 nm, R_{1y} = 9 nm, R_{1y} = 6 nm (written inside each graph).

One can observe in Fig.5 that the absolute values of the matrix elements for the transitions from the ground state to the upper six levels show clear maxima for specific transitions. It is obvious that the 1-3 transition dominates in all graphs but a strong 1-4 transition can be stimulated as is the case of the DQR configuration with

R_{1y}=9 nm and R_{2y}=36 nm. The explanation can be done based on the symmetry of the implied WFs. For instance, for the DQR configuration with R_{1y}=9 nm, R_{2y}=36 nm, $\mu_{13}=0$ and $\mu_{14}\neq 0$ because WF_1 and WF_3 (Fig.4b first row) are both antisymmetric in x variable and symmetric in y variable so the integral over x is zero. In contrast, WF_4 is symmetric both in x and y variables so the integral over x is nonzero. The analysis of the other cases can be done similarly.

Figure 6 illustrates the relative variation of the refractive index (RVRI) for the investigated cases, showing the maxima and minima and the shifts in the peaks, for certain critical values of photon energies and/or ring dimension. The regions of negative dispersion in Fig.6 are superposed over the absorbtion peaks that have a maximum where $\frac{\Delta n_r}{n_r}=0$. All these behaviors can be understood based on the correlation with the absolute dipole moments.

In Fig.6a, the amplitude of the maxima and minima of RVRI is largest for the configuration with R_{1y}=6 nm (corresponding to the largest y-width of the interior ring) followed by the value for R_{1y}=14 nm where μ_{13} takes big values. At the decrement of R_{1y}, it can be seen a blue-shift of the peaks corresponding to 1-3 transition up to R_{1y}=10 nm followed by a slight red-shift as the 1-3 transition energy first rises than decreases, as can be inferred from Fig.2a.

In Fig.6b, for the DQR structures with R_{1y}=12 nm, the amplitude of RVRI peaks is biggest for the configuration with R_{2y}=38 nm, followed closely by R_{2y}=34 nm, cases where μ_{13} is maximum. Because the 1-3 transition energy varies very slightly, the RVRI peaks are centered on 2meV with very small displacements. For the configuration with R_{2y}=32 nm (interior ring bound by an outer circle) two other peaks appears in RVRI corresponding to 1-2 and 1-6 transitions.

In Fig.6c, for the DQR structures with R_{1y}=9 nm, a maximum in the amplitude of RVRI peaks is obtained for the configuration with R_{2y}=38 nm where μ_{13} is maximum, followed by the configurations with R_{2y}=40 and 42 nm where μ_{13} has secondary maxima. The configuration with R_{2y}=36 gives RVRI peaks corresponding to 1-4 transition. RVRI is smallest for the configuration R_{2y}=32 nm.

In contrast to the other cases, for the configuration with R_{1y}=6 nm, R_{2y}=32 nm the amplitude of RVRI peaks is maximum as seen in Fig.6d. It is followed closely by the configuration with R_{2y}=38 nm because μ_{13} takes great values in these cases. For R_{2y}=40 and 42 nm the peaks of RVRI are due to 1-4 transition.

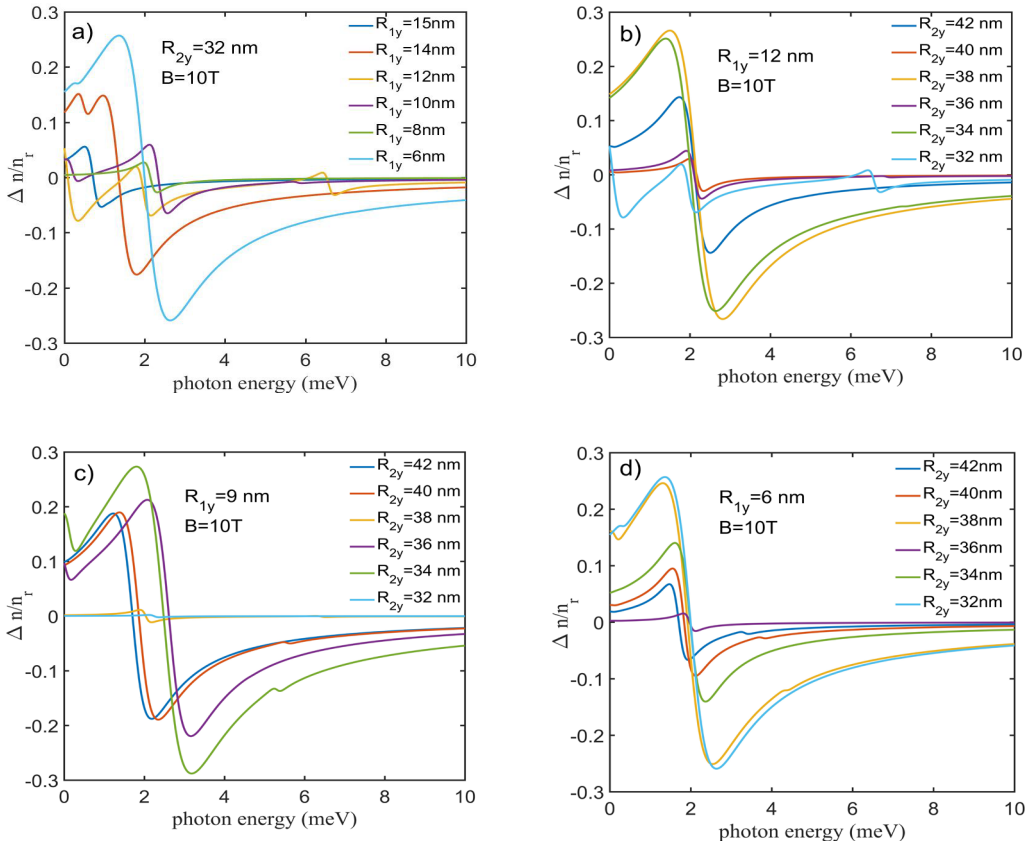

Fig. 6 The relative values of the refraction index of DQR at B=10T: (a) for different values of R_{1y} at R_{2y} = 32 nm and for different values of R_{2y} for (b) R_{1y} = 12 nm (c) R_{1y} = 9 nm (d) R_{1y} = 6 nm.

From the analysis of the relative variation of the refractive index it becomes clear that for different DQR geometry presented in each graph of Fig.6 one can choose the right configuration for an optimized response.

4. Conclusions

In this paper, we have studied the modification induced in the electronic and optical properties, by the variation of the contours of the interior ring of a GaAs/GaAlAs double quantum ring structure placed in constant, uniform magnetic field with moderate intensity (B=10 T). For the considered deformed configurations, the energy spectra show specific decreasing tendency for all the curves when R_{2y} is

increased or when R_{1y} is decreased. The energy spectra present anti-crossings that were explained in direct relationship with the wave-function symmetry exchange, due to the strong confinement of the electron in the inner ring induced by the magnetic field. The investigation of the optical properties is based on the computation of the relative variation of the refractive index in relation with the absolute dipole moments. Theoretical computations show the most probable transitions for different configurations of the DQR and offer the possibility to choose a particular value of inner ring dimensions for a desired output.

REFERENCES

[1] *V. Fomin,* Physics of Quantum Rings, 2nd ed., Springer-Verlag, Berlin Heidelberg, 2014.

[2] *T. Mano and N. Koguchi*, Nanometer-scale GaAs ring structure grown by droplet epitaxy. J. Crys. Growth **278** (2005) 108.

[3] *C. Somaschini, S. Bietti, A. Fedorov, N. Koguchi and S. Sanguinetti*, Concentric multiple rings by droplet epitaxy: fabrication and study of the morphological anisotropy. Nanoscale Res. Lett. **5** (2010) 1865.

[4] *A. Mühle, W. Wegscheider and R.J. Haug*, Coupling in concentric double quantum rings. Appl. Phys. Lett. **91** (2007) 133116.

[5] *I. Filikhin, S. Matinyan, J. Nimmo and B. Vlahovic*, Electron transfer between weakly coupled concentric quantum rings. Physica E **43** (2011) 1669.

[6] *N. Hernández, R. A. López-Doria, I. E. Rivera, et al*. Refractive index change of a D^{+2} complex in GaAs/$Al_xGa_{1-x}As$ quantum ring. J. Mater. Sci. **57** (2022) 8417.

[7] *D. Bejan, C. Stan*, Oscillatory behaviour in the energy and nonlinear optical rectification spectra of elliptic quantum rings under electric field: influence of impurity and eccentricity, Philos. Mag. **99** (2019) 492.

[8] *C. Trusca, C. Stan, and E. C. Niculescu,* Stark shift and oscillator strengths in a GaAs quantum ring with off-center donor impurity, UPB Sci. Bull. Ser. A **80** (2018) 261.

[9] *R. E. Acosta, A. L. Morales, C. M. Duque, M. E. Mora-Ramos, C. A. Duque*, Optical absorption and refractive index changes in a semiconductor quantum ring: Electric field and donor impurity effects, Phys. Status Solidi B **253** (2016) 744.

[10] *D. Nasri,* Electronic and optical properties of eccentric quantum ring under parallel magnetic field. Physica B 615 (2021) 413077.

[11] *J.I. Climente and J. Planelles,* Characteristic molecular properties of one-electron double quantum rings under magnetic fields. J. Phys. Condens. Matter **20** (2008) 035212.

[12] *F.J. Culchac, N. Porras-Montenegro and A. Latgé*, GaAs–(Ga,Al)As double quantum rings: confinement and magnetic field effects. J. Phys. Condens. Matter **20** (2008) 285215.

[13] *J. Costa e Silva, A. Chaves, G.A. Farias, M.H. Degani and R. Ferreira*, Eccentricity effects on the quantum confinement in double quantum rings. Solid State Comm. **151** (2011) 1200.

[14] *D. Bejan, C. Stan,* Electron spin and donor impurity effects on the absorption spectra of pseudo-elliptic quantum rings under magnetic field, Philos. Mag. **101** (2021) 1871.

[15] *J. Planelles, F. Rajadell and J.I. Climente*, Electron states in quantum rings with structural distortions under axial or in-plane magnetic fields. Nanotechnology **18** (2007) 375402.
[16] *D. Bejan, C. Stan*, Influence of spin–orbit interaction, Zeeman effect and light polarisation on the electronic and optical properties of pseudo-elliptic quantum rings under magnetic field, Philos. Mag. **100** (2020) 749.
[17] *D. Bejan, C. Stan, O. Toma*, Magnetic field controlled induced transparency by Autler–Townes splitting in pseudo-elliptic quantum ring, Eur. Phys. J. B **92** (2019) 153.
[18] *D. Bejan, C. Stan*, Aharonov-Bohm oscillations in pseudo-elliptic quantum rings: influence of geometry, eccentricity and electric field, Eur. Phys. J. Plus **134** (2019) 127.
[19] *D. Bejan, C. Stan, A. Petrescu-Niță*, Magnetic properties of pseudo-elliptic quantum rings: influence of impurity position and electron spin, U.P.B. Sci. Bull., Series **A 84** (2022) 163.
[20] *D. Bejan, C. Stan*, Geometry tailored magneto-optical absorption spectra of elliptically deformed double quantum rings. Philos. Mag. **102** (2022) 1755.
[21] *D. Bejan, C. Stan,* Impurity and geometry effects on the optical rectification spectra of quasi-elliptical double quantum rings, Physica E **147** (2023) 115598.
[22] COMSOL Multiphysics® v. 5.6. www.comsol.com. COMSOL AB, Stockholm, Sweden.
[23] *E. Paspalakis, J. Boviatsis, S. Baskoutas*, Effects of probe field intensity in nonlinear optical processes in asymmetric semiconductor quantum dots. J. Appl. Phys. **114** (2013) 153107.